

QSSEP describes the fluctuations of quantum coherences in the Anderson model

Ludwig Hruza^{1,2} and Tony Jin³

¹*LPENS, Département de physique, École normale supérieure, Université PSL, Sorbonne Université, Université Paris Cité, CNRS, 75005 Paris.*

²*Laboratoire de Neurosciences Cognitives et Computationnelles,*

École normale supérieure, Université PSL, INSERM, 75005 Paris, France

³*Université Côte-d'Azur, CNRS, Centrale Med, Institut de Physique de Nice, 06200 Nice, France*

Using the transfer matrix method, we numerically investigate the structure of spatial coherences and their fluctuations in the 3d Anderson model in the metallic phase when driven out-of-equilibrium by external leads at zero temperature and in linear response. We find that the stationary state entails non-local non-Gaussian correlations in the longitudinal direction, which are characteristic of diffusive non equilibrium steady states. These correlations are *quantitatively* matched, at least up to third order, by those analytically derived in the Quantum Symmetric Simple Exclusion Process (QSSEP) which describes diffusive fermions in 1d subject to *dynamical* disorder. Furthermore, the large deviation scaling and $U(1)$ invariance of these correlations imply a link between the Anderson model and free probability theory. Our findings suggest the existence of a universal structure of correlations in non-interacting diffusive quantum systems that might be captured by QSSEP.

In a seminal paper in 1995, Lee, Levitov and Yakovets [1] computed the generating function of the integrated current Q_t up to time t passing through a quasi-1d metallic wire, using a Landauer approach at low temperature and in linear response. A few years later, in 2003, Derrida, Douçot and Roche [2] managed to perform the same derivation on an entirely different model, the Symmetric Simple Exclusion Process (SSEP) [3]. Much to their surprise, they found the *exact same result*. To paraphrase them, this is anything but a trivial connection, since Lee et al. studied diffusive wires with *static disorder* on the basis of the Dorokhov-Mello-Pereyra-Kumar (DMPK) formalism [4, 5], while the computation from Derrida et al. was done on a purely classical model with *dynamical* disorder.

Not long ago, an extension of SSEP to the quantum realm named QSSEP was proposed and studied in [6, 7]. The QSSEP reproduces in mean the density and current fluctuations of the SSEP (similarly to related models [8, 9]) but additionally entails fluctuations of non-classical quantities such as quantum coherence, see Eq. (3), or entanglement. In this paper, we wish to explore further this intriguing connection by comparing the fluctuations of quantum coherence in the 3d Anderson model in the metallic regime to known analytical results from QSSEP. Another motivation to study the 3d Anderson model is that its mutual information, investigated numerically in [10], was shown to be extensive which is also the case in QSSEP as a recent exact result demonstrates [11].

Surprisingly, we find that QSSEP indeed describes *quantitatively* the fluctuations of spatial coherences in the Anderson model, at least up to third order. In particular, both models entail the presence of *non-local non-Gaussian* correlations which are characteristic of the non-equilibrium steady state (NESS) of diffusive systems. This brings forth the exciting possibility that QSSEP provides an effective description of diffusive metallic

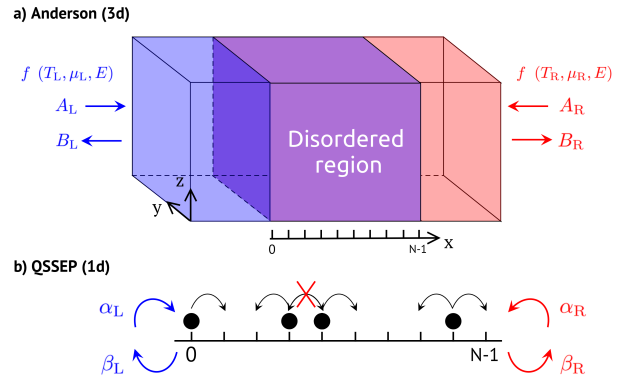


FIG. 1. The two models investigated in this paper. **a)** The Anderson model in 3d. Electrons propagate from the leads (clean regions) denoted left/right (L/R) through a region with *static* disordered potential in purple. The leads are taken at thermal equilibrium with Fermi distributions $f(T_{L/R}, \mu_{L/R}, E)$. Here $A_{R/L}$ denotes the incoming modes and $B_{R/L}$ the outgoing ones. **b)** The Quantum Symmetric Simple Exclusion Process (QSSEP) in 1d. The system is driven out-of-equilibrium by Lindblad boundary terms injecting and extracting particles at respective rates $\alpha_{L/R}$, $\beta_{L/R}$. The bulk dynamics is given by Eq. (2) and models fermions undergoing coherent jumps with random amplitudes both in time *and* space.

wires. As the statistics of QSSEP was recently connected to free probability theory [12, 13], our finding suggests the existence of a hidden free probability structure in the NESS of diffusive metallic wires [14].

Both in a 3d and quasi-1d geometry, the shape of the spatial correlations in the Anderson model is accurately captured by QSSEP. However the correct scaling with system size only matches in 3d. We leave the interesting discussion of the quasi-1d case to the SM [15].

We begin by presenting the models and recall some useful results and methodology. We then present our numerical results concerning the Anderson model

and show their quantitative agreements with the exact known results from QSSEP. Finally, we propose some elements and a roadmap for proving the correspondence analytically. We conclude by discussing exciting open questions.

Anderson model [16]. We consider the Hamiltonian

$$H_A := - \sum_{(i,j) \text{ neighbors}} \left(t_{(i,j)} c_i^\dagger c_j + \text{h.c.} \right) + \sum_i V_i c_i^\dagger c_i \quad (1)$$

where $\mathbf{i} := (i_x, i_y, i_z)$, $t_{(i,j)} = t_{x/y/z}$ for a link in the $x/y/z$ direction and c_i is the usual fermionic annihilation operator, see Fig. 1 a. The random onsite-potentials V_i are i.i.d. and uniform in $[-\frac{W}{2}, \frac{W}{2}]$ inside a cubic disordered region of size N^3 . On the boundaries in x -direction ($i_x = 0, N-1$), we attach clean infinite leads ($W = 0$) to the system which are described by Fermi distributions $f(T_\alpha, \mu_\alpha, E)$, where $\alpha = L, R$ denotes the left and right lead. The dispersion relation in the leads is given by $E_{\mathbf{k}} = -\sum_{\nu=x,y,z} 2t_\nu \cos(k_\nu a)$ with $\mathbf{k} := (k_x, \frac{2\pi n}{Na}, \frac{2\pi m}{Na})$, n, m integers $\in [0, N-1]$, a the lattice spacing and $k_x \in [-\frac{\pi}{a}, \frac{\pi}{a}]$ a continuous index, as the total system is infinite in the x -direction. Note that fixing $E_{\mathbf{k}}$ and transverse momenta $k_\perp := (k_y, k_z)$ fixes $k_x(E, k_\perp)$. On each side, we denote $A_\alpha(E, k_\perp)$ the amplitudes of the incoming and $B_\alpha(E, k_\perp)$ the amplitudes of the outgoing plane waves with given energy and transverse momentum. Since the system is non-interacting, we can describe the NESS using Landauer-Büttiker's formalism [17, 18].

This model has a well-known phase transition from a metallic to a localized phase as W is increased above a critical value W_c [19]. We will work in the metallic phase $W_c < W$. Additionally, we are interested in the regime where the mean-free path ℓ is small compared to the total system size $\ell \ll Na$.

QSSEP. The Quantum Symmetric Simple Exclusion Process was introduced in [20] and subsequently studied in [6, 7, 11–13, 21–23]. The QSSEP describes random hopping of fermionic particles on a discrete 1d lattice coupled to boundary reservoirs on each side. This model is explicitly diffusive, i.e. it fulfills Fick's law at the operatorial level. Remarkably, it is possible to obtain all the spatial connected correlations for the out-of-equilibrium stationary state *at any order* in this model. The bulk Hamiltonian is given by (see Fig. 1 b)

$$dH_{\text{QSSEP}}(t) := \sqrt{D} \sum_{i=0}^{N-2} c_i^\dagger c_{i+1} dW_t^i + \text{h.c.} \quad (2)$$

where $W_t^i := \frac{B_t^{1,i} + iB_t^{2,i}}{\sqrt{2}}$ with $B_t^{1,i}$ and $B_t^{2,i}$ independent Brownian processes with variance $\delta_{ij}t$, and D the diffusion constant. The density matrix evolves according to $\rho_{t+dt} = e^{-idH_t} \rho_t e^{idH_t}$. Additionally, the system is driven out-of-equilibrium by Lindblad creation

and annihilation superoperators $\mathcal{D}[c^\dagger/c]$ acting on the boundaries with rates $\alpha_{L/R}$ for the creation and $\beta_{L/R}$ for the annihilation. For simplification, we will fix $\alpha_{L/R} + \beta_{L/R} = 1$ throughout the manuscript. In the absence of bulk dynamics, the effect of the boundary terms is to fix the density of the first site to α_L and of the last site to α_R .

There are 3 types of disorder we will consider in the problem. In what follows, we denote quantum averages in both models by $\langle \bullet \rangle$, static disorder average in Anderson with \bullet , and average with respect to the fluctuating complex noise in QSSEP by $\mathbb{E}[\bullet]$.

QSSEP correlations. We recall here relevant results on the spatial coherences of QSSEP in the NESS [24]. We are interested in the two-point function

$$G_{ij} := \text{tr} \left(\rho_{t=\infty} c_j^\dagger c_i \right) \quad (3)$$

and its fluctuations with respect to the noise. Because the dynamics preserves Gaussian fermionic states for each individual stochastic trajectory, the statistics of QSSEP is fully encoded in G_{ij} . The cumulants of G_{ij} satisfy a $U(1)$ invariance, i.e. $\mathbb{E}[G_{i_1 j_1} \cdots G_{i_n j_n}]^c$ is non-zero only if $\{j_1, \dots, j_n\}$ is a permutation of $\{i_1, \dots, i_n\}$. Of all possible allowed cumulants, so-called ‘‘cyclic cumulants’’ $\mathbb{E}[G_{i_1 i_2} G_{i_2 i_3} \cdots G_{i_n i_1}]^c$ are of special importance: They scale as N^{1-n} with the number of sites N and they constitute the leading order cumulant at any order n . In the limit $N \rightarrow \infty$, with coordinates $x_k := \frac{i_k}{N} \in [0, 1]$, we define

$$g_n^Q(x_1, \dots, x_n) := \lim_{N \rightarrow \infty} N^{n-1} \mathbb{E}[G_{i_1 i_2} G_{i_2 i_3} \cdots G_{i_n i_1}]^c \quad (4)$$

with $\Delta n = \alpha_R - \alpha_L$ the boundary imbalance. These functions contain the complete information about QSSEP at leading order in N . The first three orders are

$$\begin{aligned} g_1^Q &= \Delta n x, & g_2^Q &= (\Delta n)^2 (\min(x, y) - xy), \\ g_3^Q &= (\Delta n)^3 (\min(x, y, z) - (x \min(y, z))_{\odot 3} + 2xyz) \end{aligned} \quad (5)$$

and $(\cdots)_{\odot 3}$ denotes a sum of three terms obtain by cyclic permutation of (x, y, z) . Note that these quantities are completely independent of the diffusion constant D .

Thanks to an elegant connection between QSSEP and free probability [12, 13], the general solution can be formulated recursively as

$$\sum_{\pi \in \text{NC}(n)} \prod_{p \in \pi} g_{|p|}^Q(\vec{x}_p) = (\Delta n)^n \min(x_1, \dots, x_n) \quad (6)$$

with $\pi \in \text{NC}(n)$ a non-crossing set-partition of n elements, p the parts of this partition, $|p|$ the number of elements in part p and $\vec{x}_p = (x_i)_{i \in p}$.

Numerical results for the Anderson model. We now present numerical results obtained in the 3d Anderson model and will compare them with the exact

results for the QSSEP. Our approach relies on the Landauer-Büttiker formalism [17, 25] and the transfer matrix method for non-interacting fermionic systems [19, 26, 27] which we recall in the SM [15]. The numerics allows us to access single-particle eigenstates corresponding to particles incoming from lead $\alpha = L, R$ with energy E and transverse momentum k_\perp which we denote $|\psi_{\alpha, E, k_\perp}\rangle$. Let $a_{\alpha, E, k_\perp}^\dagger$ be the second quantized fermionic creation operator associated to $|\psi_{\alpha, E, k_\perp}\rangle$. We fix the statistics of the bath by $\langle a_{\alpha, E, k_\perp}^\dagger a_{\alpha', E', k'_\perp} \rangle = \delta_{\alpha\alpha'} \delta(E, E') \delta_{k_\perp, k'_\perp} f(T_\alpha, \mu_\alpha, E)$. The two-point function $G_{ij}^A := \langle c_j^\dagger c_i \rangle$ whose statistics we are interested in is

$$G_{ij}^A = \int dE \sum_{\alpha=L,R} f(T_\alpha, \mu_\alpha, E) \sum_{k_\perp} \psi_{\alpha, E, k_\perp}^*(\mathbf{j}) \psi_{\alpha, E, k_\perp}(\mathbf{i}).$$

Imposing a small imbalance $\mu_{L/R} = \mp \delta\mu$ between the leads and fixing $T_L = T_R = 0$, we can expand around $E = 0$. Replacing the Fermi distributions f by step functions and denoting $G_{ij}^{\alpha}(E) := \sum_{k_\perp} \psi_{\alpha, E, k_\perp}^*(\mathbf{j}) \psi_{\alpha, E, k_\perp}(\mathbf{i})$,

$$G^A \approx \delta\mu(G^R(0^+) - G^L(0^-)) + \int_{-\infty}^0 dE(G^R(E) + G^L(E))$$

and one identifies the non-equilibrium part of G^A as

$$G^{\text{neq}} := \delta\mu(G^R(0^+) - G^L(0^-)), \quad (7)$$

where 0^\pm means that we can evaluate the energy for any point in the interval $(0, \pm\delta\mu]$. In our simulations we take $0^\pm = \pm 0.2$. For convenience, we will avoid dealing with imaginary values of k_x by imposing an anisotropic tight-binding term with $t_y, t_z < \frac{1}{2}t_x$. Here we choose $t_x = 1$ and $t_y = t_z = 0.4$. We conventionally fix the rate of incoming particle of a given mode to 1 and $\delta\mu = 1$. We fix the disorder strength W (in the metallic regime) a posteriori to best fit the QSSEP prediction. At second order, we will see that this is the case for $W \approx 6$. Other values of W for which the agreement is worse are shown in the SM [15].

We will now define correlations functions g_n^A for the Anderson model in analogy to g_n^Q for QSSEP and numerically investigate to what extent they agree, i.e.

$$g_n^A \stackrel{?}{=} g_n^Q. \quad (8)$$

where the imbalance Δn in the definition of g_n^Q is taken as a fitting parameter. Our proposal is to define

$$g_n^A(x_1, \dots, x_n) := N^{n-1} \left[\overline{G_{i_1 i_2}^{\text{neq}} \dots G_{i_n i_1}^{\text{neq}}} \right]_\perp \quad (9)$$

with $x_k = i_{k,x}/N$ the rescaled positions. Here $\overline{\bullet}$ denotes the connected disorder average and $[\bullet]_\perp$ denotes the spatial average over perpendicular indices, which reduces the formerly 3d expression to 1d

$$\left[G_{i_1 i_2}^{\text{neq}} \dots G_{i_n i_1}^{\text{neq}} \right]_\perp := \frac{1}{N^{2n}} \sum_{i_{1\perp}, \dots, i_{n\perp}} G_{i_1 i_2}^{\text{neq}} \dots G_{i_n i_1}^{\text{neq}} \quad (10)$$

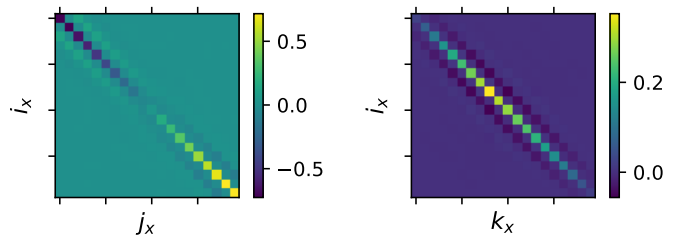


FIG. 2. Numerical verification of the $U(1)$ invariance of cumulants in the Anderson model for $W = 6$ and $N = 20$. Left: $\left[G_{ij}^{\text{neq}} \right]_{\perp}$ (with $i_{\perp} = j_{\perp}$) is nonzero only if $i_x = j_x$. Right: $N \left[G_{ij}^{\text{neq}} G_{jk}^{\text{neq}} \right]_{\perp}$ (with $i_{\perp} = k_{\perp}$ and $j_x = 8$) requires $i_x = k_x$.

with $i_{\perp} = (i_y, i_z)$. Note that (9) is $U(1)$ invariant by construction. We numerically verify in Fig. 2 that non-vanishing cumulants of coherences in the Anderson model must be $U(1)$ invariant. Importantly, this $U(1)$ invariance, together with the large deviation scaling (9), implies a link between the Anderson model and free probability theory [13].

We conduct investigation of Eq. (8) up to order $n = 3$. $n=1$. We plot g_1^A in Fig. 3 a. The local density linearly interpolates between the right and left boundary, as expected for a diffusive system. Fitting the slope, we get $\Delta n^{(1)} = 1.71$.

$n=2$. Results for g_2^A are shown in Fig. 3 b,c and are compared to g_2^Q for QSSEP from Eq. (5). In Fig. 3 c, the value $\Delta n^{(2)}$ is obtained by extrapolating the numerical data to $N \rightarrow \infty$ using the ansatz $g_2^A = g_2^Q \left(1 + \frac{\beta}{(\Delta n^{(2)})^2 N} + \frac{\gamma}{(\Delta n^{(2)})^2 N^2} \right)$ and β, γ additional fitting parameters. We obtain $\Delta n^{(2)} = 1.43$ which is slightly below $\Delta n^{(1)}$. Ideally, the two values would agree.

$n=3$. Finally, we show g_3^A in Fig. 3 d,e,f. The correspondence is less clear than for the second order but still in good qualitative agreement. The optimal fit for the density imbalance is $\Delta n^{(3)} = -0.77$ which is way below the first and second order values and maybe more significantly, carries a negative sign. Additionally, we see significant discrepancies whenever the indices are brought close together, such as in Fig. 3 f.

Additionally, in Fig. 4 we checked for different W if the system size scaling of the second and third cumulants is the one predicted by QSSEP. We find best agreement for $W \in [5, 6]$ which is consistent with $W = 6$ for which also the shape of g_n^A matches best with QSSEP (see Fig. 3).

Hints for a proof. Here we provide preliminary ideas for a proof of the correspondence. First, note that the pure random dephasing model,

$$dH_{\text{Deph}}(t) = H_0 + \sqrt{\gamma} \sum_i n_i dB_t^i, \quad (11)$$

where H_0 is the usual fermionic tight-binding model and B_t^i are independent Brownian motions at every site,

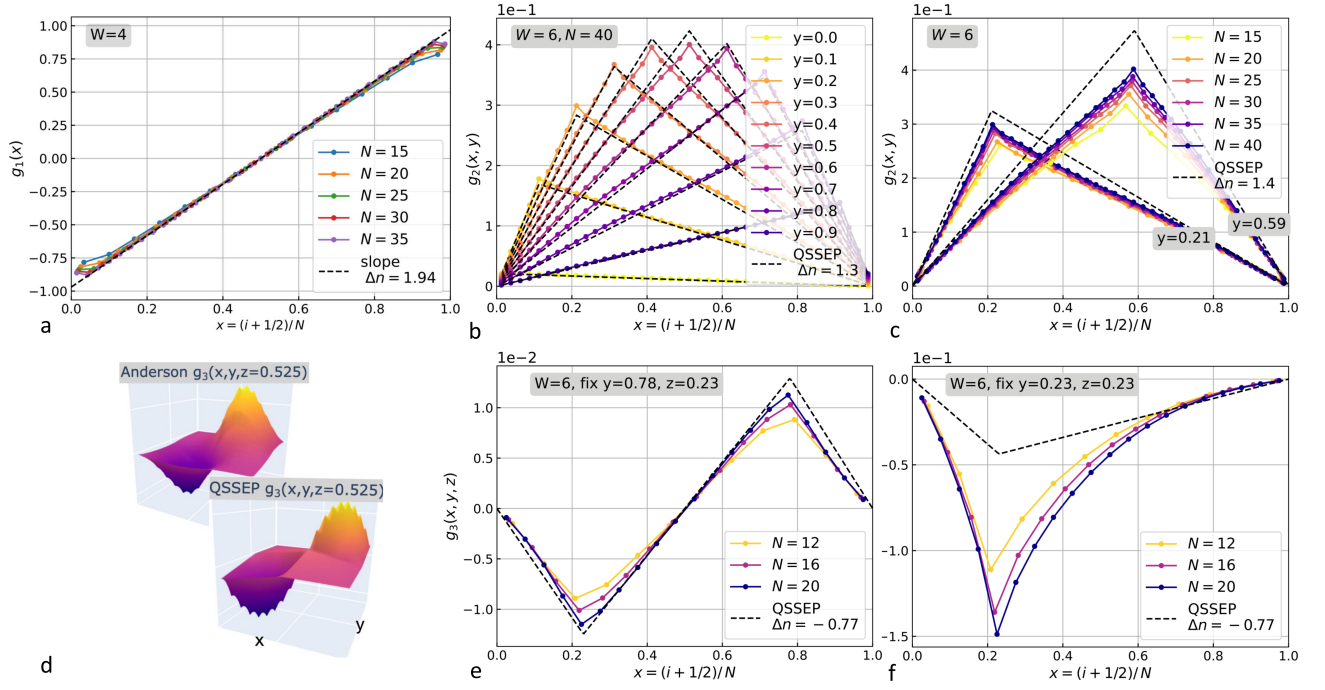


FIG. 3. On all the figures, the dashed line corresponds to analytical predictions from QSSEP (5) while the solid colored lines correspond to numerical simulations of the 3d Anderson model for different linear sizes N and disorder $W = 6$. We use the continuous notations for coordinates in x -direction, $x = \frac{i_x}{N}$, $y = \frac{j_x}{N}$ and $z := \frac{k_x}{N}$. The disorder averages are performed over 1000 realizations for every point. **a)** The density $g_1^{Q/A}$ is linear as expected for diffusive systems. Its slope is $\Delta n^{(1)} = 1.75$. **b)** Comparison of the second cumulant $g_2^{Q/A}$ between QSSEP and Anderson for $N = 40$. The different curves correspond to different values of y . The agreement with QSSEP is very good with $\Delta n^{(2)} = 1.3$ obtained as the best fit to the data. **c)** Same plot, but collapsing different values of N , which nicely converge for increasing N . The imbalance $\Delta n^{(2)} = 1.4$ for the QSSEP prediction is obtained as a fit to an extrapolation of the data to $N = \infty$. **d)** 3d plots of the third cumulant in both models for a cut at $z = 0.525$ show a qualitative agreement of the two shapes. **e,f)** Cuts of $g_3^{Q/A}$ for fixed $z = 0.23$ and $y = 0.78, 0.23$. The imbalance $\Delta n^{(3)} = -0.77$ here is fitted by hand to the cut with $y = 0.78$. The agreement with QSSEP at the given imbalance is much worse for $y = 0.23$. A reason could be that here the values of y and z coincide. Notice the *negative* sign for $\Delta n^{(3)}$.

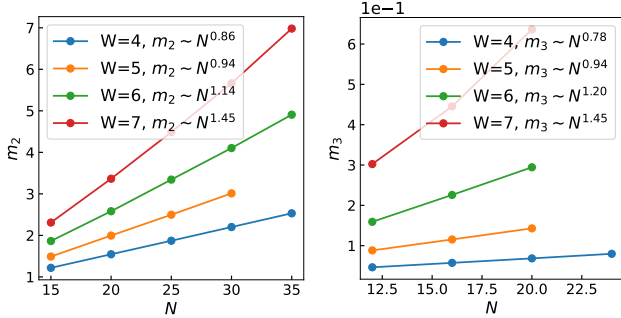


FIG. 4. Scaling of the correlations of coherences with system size in the 3d Anderson model. Here $m_2 := \sum_{i_x j_x} \left[G_{ij}^{\text{neq}} G_{ji}^{\text{neq}c} \right]_{\perp}$, $m_3 := \sum_{i_x j_x, k_x} \left[G_{ij}^{\text{neq}} G_{jk}^{\text{neq}} G_{ki}^{\text{neq}c} \right]_{\perp}$. For values in the interval $W \in [5, 6]$, both expressions scale approximately proportional to N as predicted by QSSEP, since cyclic cumulants of order n should scale with N^{1-n} .

maps *exactly* to the QSSEP when considering the strong dephasing, long time limit $\gamma \rightarrow \infty$, $t \rightarrow \infty$, $s := \frac{t}{\gamma}$ finite, where s plays the role of an effective time [20].

This model has been thoroughly studied in the literature, see e.g. [20, 28–34], some of the motivations being its analytical tractability and the fact that it entails *diffusive* transport in 1d. One can suppose that this mapping will still be valid at finite γ but large space and time scales, in some renormalization group sense that has yet to be made precise.

Under this assumption, we are left with understanding how a dynamical noise (11) may generate the same statistical fluctuations as static disordered (1). One possible route is to examine the diagrammatic structure of field theories of both models. At the single replica level, a way to resum the diagrammatic series for the self-energy is the well-known *self-consistent Born approximation* (SCBA) [35, 36]. For the Anderson model, this approximation is justified for $(k_F \ell)^{d-1} \gg 1$, i.e for $d > 1$ and in the mesoscopic limit. Under this assumption, the imaginary part of the self-energy can be computed in the continuum. In 3d, it is $\Im(\Sigma) \approx \left(\frac{t_x}{t_{\perp}} \right) \nu(E_F) \mathcal{W}^2$ where $\mathcal{W} := a^{3/2} W$ and ν is the density of states. From the self-energy, one deduces the

scattering time $\tau \propto \Im(\Sigma)^{-1}$ and subsequently the mean free path $\ell \propto v_F \tau$ and the diffusion constant $D \propto v_F \tau$.

On the other hand, it turns out that for the dephasing model, the SCBA is *exact* [33, 37] which is a direct consequence of the fact that the noise term is delta correlated in time. The self-energy in 1d was computed to be $\Im(\Sigma) \propto \gamma$. Thus, at the one replica level, the two theories match when identifying

$$\gamma \rightarrow \left(\frac{t_z}{t_\perp}\right) \nu(E_F) \mathcal{W}^2. \quad (12)$$

Improving this statement would require to look at higher order cumulants of G . For the second cumulant, one would need to analyze the Bethe-Salpeter equations [38] and search for a diagrammatic correspondence between the models. We leave this to a subsequent study.

Conclusion. We first emphasize some delicate points. The correspondence for the fluctuations of the integrated current Q_t between SSEP and diffusive conductors by Derrida et al. [2] is valid in a *quasi-1d* geometry. In contrast, the extensive scaling of the quantum mutual information in the Anderson model [10] is only valid in *3d*. In our study, we found an agreement of the shape of correlations with QSSEP both in 3d and quasi-1d [15], but the scaling with system size only matches in 3d. This is to some extent paradoxical, since the statistics of SSEP is already contained in QSSEP. Furthermore, the optimal disorder ($W = 6$) corresponds to the mean free path of the order of the lattice spacing [39], which suggests that no coarse-graining in the longitudinal direction would be necessary for QSSEP to emerge, at least for cumulants at order 1 and 2.

To sum up, we have shown that, despite fundamental disparities between the Anderson model and the QSSEP, the fluctuations of quantum correlations up to third order in both models are analogous, modulo an adjustment of the imbalance Δn at every order. This unexpected correspondence hints at the existence of a universal correlation structure in out-of-equilibrium quantum diffusive systems. The possibility that free probability plays a central role in this universal structure opens an exciting avenue of exploration. A key question is if the correspondence with QSSEP discussed here can be extended to other models, and ultimately, to formulate a quantum version of the macroscopic fluctuation theory (MFT) [40]. We note that encouraging steps in this endeavor have been made recently with numerical simulations in random unitary circuits [41] and experiments in chaotic cold atoms systems [42] showing that the classical MFT was able to describe these systems.

Acknowledgments. The authors extend their gratitude to Denis Bernard for past and present collaborations and ongoing encouragement. We are thankful towards Marko Medenjak and Alexios Michailidis for initial collaboration on this subject. We thank Mathias Albert and Christian

Miniatura for illuminating discussions on the Anderson model. Part of this collaboration was conducted in the “Les Gustins” summer school.

-
- [1] H. Lee, L. S. Levitov, and A. Y. Yakovets, Phys. Rev. B **51**, 4079 (1995).
 - [2] B. Derrida, B. Douçot, and P.-E. Roche, Journal of Statistical Physics **115**, 717 (2004).
 - [3] B. Derrida, Journal of Statistical Mechanics: Theory and Experiment **2007**, 07023 (2007), arXiv:cond-mat/0703762 [cond-mat.stat-mech].
 - [4] O. Dorokhov, Pis'ma Zh. Eksp. Teor. Fiz. **36**, 259 (1982).
 - [5] P. Mello, P. Pereyra, and N. Kumar, Annals of Physics **181**, 290 (1988).
 - [6] M. Bauer, D. Bernard, and T. Jin, SciPost Phys. **6**, 45 (2019).
 - [7] D. Bernard and T. Jin, Phys. Rev. Lett. **123**, 080601 (2019).
 - [8] V. Eisler, Journal of Statistical Mechanics: Theory and Experiment **2011**, 06007 (2011), arXiv:1104.4050 [cond-mat.stat-mech].
 - [9] K. Temme, M. M. Wolf, and F. Verstraete, New Journal of Physics **14**, 075004 (2012).
 - [10] M. J. Gullans and D. A. Huse, Phys. Rev. X **9**, 021007 (2019).
 - [11] D. Bernard and L. Hruza, SciPost Physics **15**, 10.21468/scipostphys.15.4.175 (2023).
 - [12] P. Biane, Ann. Inst. Henri Poincaré Comb. Phys. Interact. 10.4171/AIHPD/175 (2023), arXiv:2111.12403.
 - [13] L. Hruza and D. Bernard, Phys. Rev. X **13**, 011045 (2023).
 - [14] An obvious but important point to mention is that this mapping, if it were to exist, can not hold in a generic matter. For instance, it is known that, contrarily to the Anderson model, there is no localized phase for the QSSEP model. We thus restrict our conjecture to the metallic phase of the 3d Anderson model.
 - [15] Supplemental Material.
 - [16] P. W. Anderson, Phys. Rev. **109**, 1492 (1958).
 - [17] R. Landauer, IBM Journal of Research and Development **1**, 223 (1957).
 - [18] M. Büttiker, Phys. Rev. Lett. **57**, 1761 (1986).
 - [19] P. Markoš, Acta Physica Slovaca. Reviews and Tutorials **56**, 10.2478/v10155-010-0081-0 (2006).
 - [20] M. Bauer, D. Bernard, and T. Jin, SciPost Phys. **3**, 033 (2017).
 - [21] D. Bernard and T. Jin, Communications in Mathematical Physics **384**, 1141 (2021).
 - [22] D. Bernard and L. Piroli, Phys. Rev. E **104**, 014146 (2021).
 - [23] D. Bernard, F. H. L. Essler, L. Hruza, and M. Medenjak, SciPost Phys. **12**, 042 (2022).
 - [24] It is also possible to make statements about the dynamics of QSSEP [13], but here we restrict ourselves to the steady state.
 - [25] M. Büttiker, Y. Imry, R. Landauer, and S. Pinhas, Phys. Rev. B **31**, 6207 (1985).
 - [26] A. MacKinnon and B. Kramer, Zeitschrift für Physik B Condensed Matter **53**, 1 (1983).
 - [27] J. Pendry, A. MacKinnon, and P. Roberts, Proceedings of

- the Royal Society of London. Series A: Mathematical and Physical Sciences **437**, 10.1098/rspa.1992.0047 (1992).
- [28] M. Žnidarič, *Journal of Statistical Mechanics: Theory and Experiment* **2010**, L05002 (2010).
- [29] M. Žnidarič, *Phys. Rev. E* **83**, 011108 (2011).
- [30] M. Žnidarič and M. Horvat, *The European Physical Journal B* **86**, 67 (2013).
- [31] M. V. Medvedyeva, F. H. L. Essler, and T. Prosen, *Phys. Rev. Lett.* **117**, 137202 (2016).
- [32] A. Bastianello, J. De Nardis, and A. De Luca, *Phys. Rev. B* **102**, 161110 (2020).
- [33] P. E. Dolgirev, J. Marino, D. Sels, and E. Demler, *Phys. Rev. B* **102**, 100301 (2020).
- [34] T. Jin, J. S. Ferreira, M. Filippone, and T. Giamarchi, *Physical Review Research* **4**, 10.1103/physrevresearch.4.013109 (2022).
- [35] M. Born, *Zeitschrift für Physik* **38**, 803 (1926).
- [36] A. Altland and B. D. Simons, *Condensed Matter Field Theory* (Cambridge University Press, 2010).
- [37] T. Jin, M. Filippone, and T. Giamarchi, *Phys. Rev. B* **102**, 205131 (2020).
- [38] P. A. Lee and T. V. Ramakrishnan, *Rev. Mod. Phys.* **57**, 287 (1985).
- [39] E. N. Economou, C. M. Soukoulis, and A. D. Zdetsis, *Phys. Rev. B* **31**, 6483 (1985).
- [40] D. Bernard, *Journal of Physics A: Mathematical and Theoretical* **54**, 433001 (2021).
- [41] E. McCulloch, J. De Nardis, S. Gopalakrishnan, and R. Vasseur, *Phys. Rev. Lett.* **131**, 210402 (2023).
- [42] J. F. Wienand, S. Karch, A. Impertro, C. Schweizer, E. McCulloch, R. Vasseur, S. Gopalakrishnan, M. Aidelsburger, and I. Bloch, Emergence of fluctuating hydrodynamics in chaotic quantum systems (2023), arXiv:2306.11457 [cond-mat.quant-gas].
- [43] P. A. Mello and A. D. Stone, *Phys. Rev. B* **44**, 3559 (1991).
- [44] R. A. Jalabert and J.-L. Pichard, *Journal de Physique I* **5**, 287–324 (1995).

SUPPLEMENTAL MATERIAL

Results for the quasi-1d Anderson model

While all results presented in the main text deal with the the 3d Anderson model in a cubic geometry (that is $N_x = N_y = N_z$), here we present the results for the quasi-1d case where the longitudinal dimension $N_x \gg N_y, N_z$ is much greater than the transverse dimensions. This is the regime in which the result of Lee et. al [1] is valid, since they assume that the transmission properties of each channel (i.e. each perpendicular mode k_\perp) are statistically independent. The same assumption also allows for analytic calculations via the DMPK equation [4, 5, 43]. In contrast to this, in a recent numerical study of entanglement in the Anderson model, Gullans and Huse [10] have shown that the mutual information scales extensively with the volume only in the 3d case, but not in quasi-1d. This is because channels in the 3d case are no longer independent [44]. Keeping in mind that also in QSSEP the mutual information scales as the volume [11], we expected that the quasi-1d regime would be the wrong place to look for a correspondence with QSSEP. Much to our surprise, we find that, besides a wrong scaling with the longitudinal dimension N_x (where N_y and N_z stay fixed), the shape of correlations of coherences matches QSSEP.

To show this, we first define the transverse spatial average in analogy to the main text as

$$[G_{i_1 i_2}^{\text{neq}} \cdots G_{i_n i_1}^{\text{neq}}]_\perp := \frac{1}{(N_y N_z)^n} \sum_{i_{1\perp}, \dots, i_{n\perp}} G_{i_1 i_2}^{\text{neq}} \cdots G_{i_n i_1}^{\text{neq}}. \quad (13)$$

with $i_\perp = (i_y, i_z)$ and then define the rescaled cumulants of coherences as

$$g_n^{\text{quasi-1d}}(x_1, \dots, x_n) := \frac{1}{N_x^{n-1}} \left[\overline{G_{i_1 i_2}^{\text{neq}} \cdots G_{i_n i_1}^{\text{neq}}} \right]_\perp \quad (14)$$

with $x_k = i_{k,x}/N_x$ and $\overline{\cdots}^c$ the connected disorder average. In contrast to Eq. (9), here we divide rather than multiply by N_x^{n-1} . Fig. 5 confirms the new scaling with N_x which is best respected for $W \approx 4$. Figs. 6 and 7 show the numerical results for the second and third cumulants, respectively. The match with QSSEP is best for $W \approx 5$, though convergence of the curves for different N_x is not as good as for $W = 2$. This could be caused by numerical imprecisions which become more important for greater W .

Note that all the cumulants of G^{neq} are upper bounded since $|G_{ij}^{\text{neq}}| \leq 1$. Consequently, this scaling with N_x must break down eventually. We expect this to occur when $N_x \gg \xi$ with ξ the localization length, which is the condition to be in the localized regime.

To conclude, we comment on the trace of the $(N_x N_y N_z) \times (N_x N_y N_z)$ matrix G^{neq} and its scaling with N_x ,

$$\overline{\text{Tr}(G^{\text{neq}})^n} = \sum_{i_{1x}, \dots, i_{nx}} (N_y N_z)^n \left[\overline{G_{i_1 i_2}^{\text{neq}} \cdots G_{i_n i_1}^{\text{neq}}} \right]_\perp \sim \begin{cases} N_x^{2n-1} (N_y N_z)^n, & \text{quasi-1d} \\ N_x^{2n+1}, & \text{3d with } N_x = N_y = N_z. \end{cases} \quad (15)$$

This suggests, that in terms of scaling with system size, the correlations of coherences in 3d are stronger than in quasi-1d. Why QSSEP still captures the shape of those correlations in both cases remains a riddle to us.

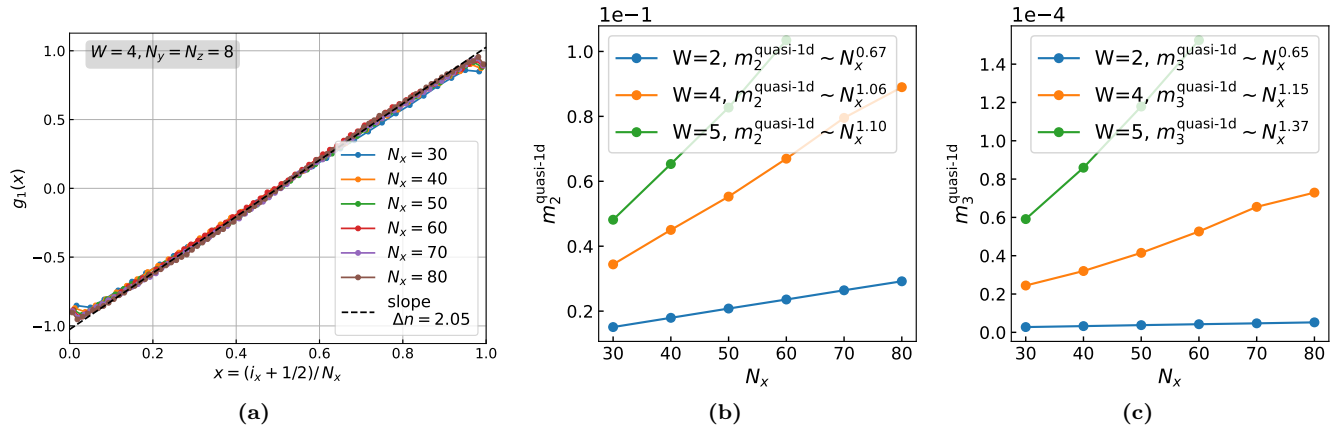


FIG. 5. (a) First cumulant (or density) $g_1^{\text{quasi-1d}}(x) = \left[G_{ii}^{\text{neq}} \right]_{\perp}$ in the quasi-1d Anderson model for $W = 4$ with fixed transverse dimensions $N_y = N_z = 8$. In all plots we shift the continuous coordinate $x = i_x/N_x$ by $1/(2N_x)$ to center the data within the interval $[0, 1]$ keeping in mind that $i_x = 0, \dots, N_x - 1$. (b) and (c) The scaling with N_x assumed in the definition of $g_n^{\text{quasi-1d}}$ is confirmed for $W \approx 4$ since $m_2^{\text{quasi-1d}} := \frac{1}{N_x^2} \sum_{i_x, j_x} \left[G_{ij}^{\text{neq}} G_{ji}^{\text{neqc}} \right]_{\perp}$ and $m_3^{\text{quasi-1d}} := \frac{1}{N_x^4} \sum_{i_x, j_x, k_x} \left[G_{ij}^{\text{neq}} G_{jk}^{\text{neqc}} G_{ki}^{\text{neqc}} \right]_{\perp}$ scale approximately linearly with N_x . All data points are obtained as averages over 500 samples.

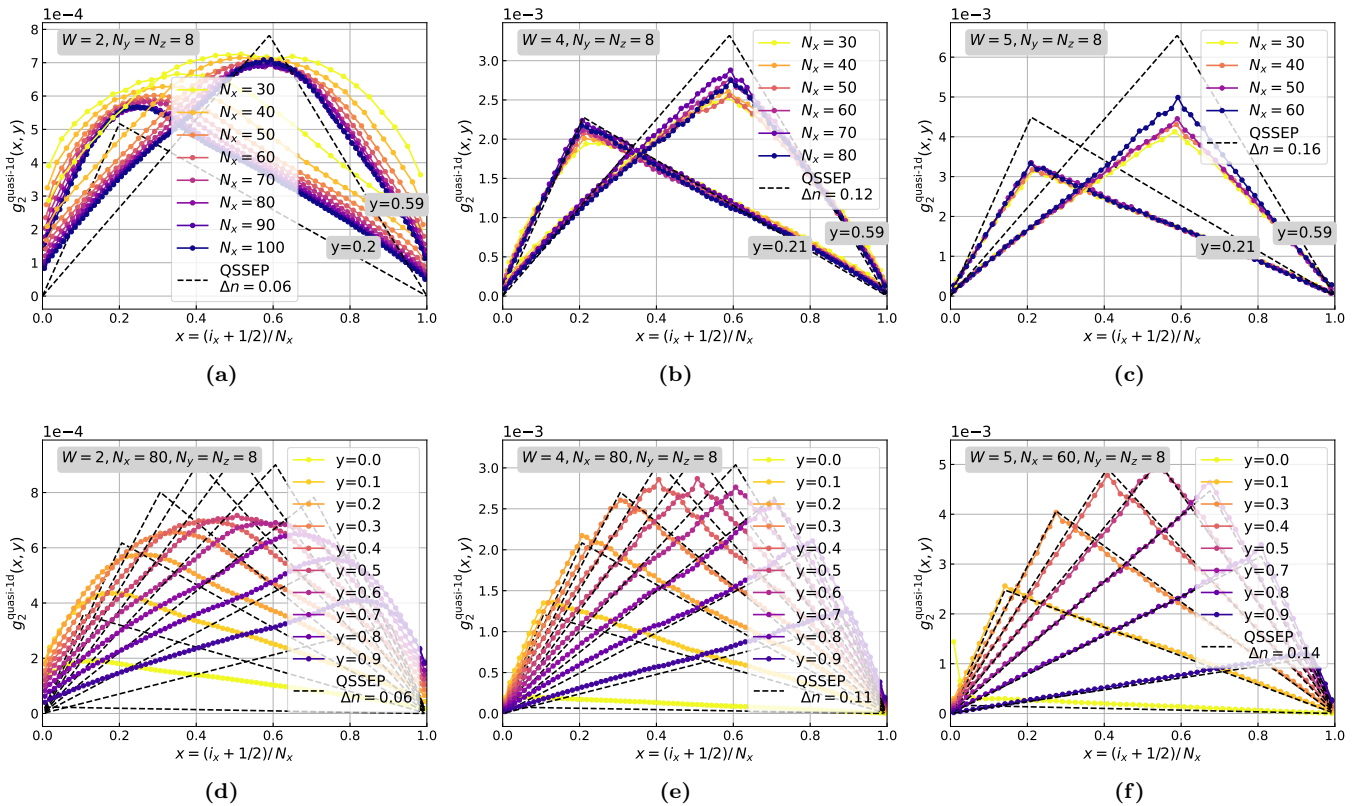


FIG. 6. Second cumulant $g_2^{\text{quasi-1d}}(x, y)$ in the quasi-1d Anderson model for $W = 2, 4, 5$ and with fixed transverse dimensions $N_y = N_z = 8$. In (a)-(c) curves for two fixed values of $y = j_x/N_x = 0.21, 0.59$ and for different values of the longitudinal dimension N_x are collapsed in order to show that the curves converge for large N_x . We observe that convergence is better for lower values of W . The value of Δn for the QSSEP prediction (dashed line) is found as the best fit to an extrapolation of the data to $N_x \rightarrow \infty$. In (d)-(f) curves correspond to a single value of N_x but at different values of y . The value of Δn for the QSSEP prediction (dashed line) is obtained as the best fit to the data for the corresponding value N_x (and not for $N_x \rightarrow \infty$). Note that the correspondence with QSSEP is best for $W = 5$. All data points are obtained as averages over 500 samples.

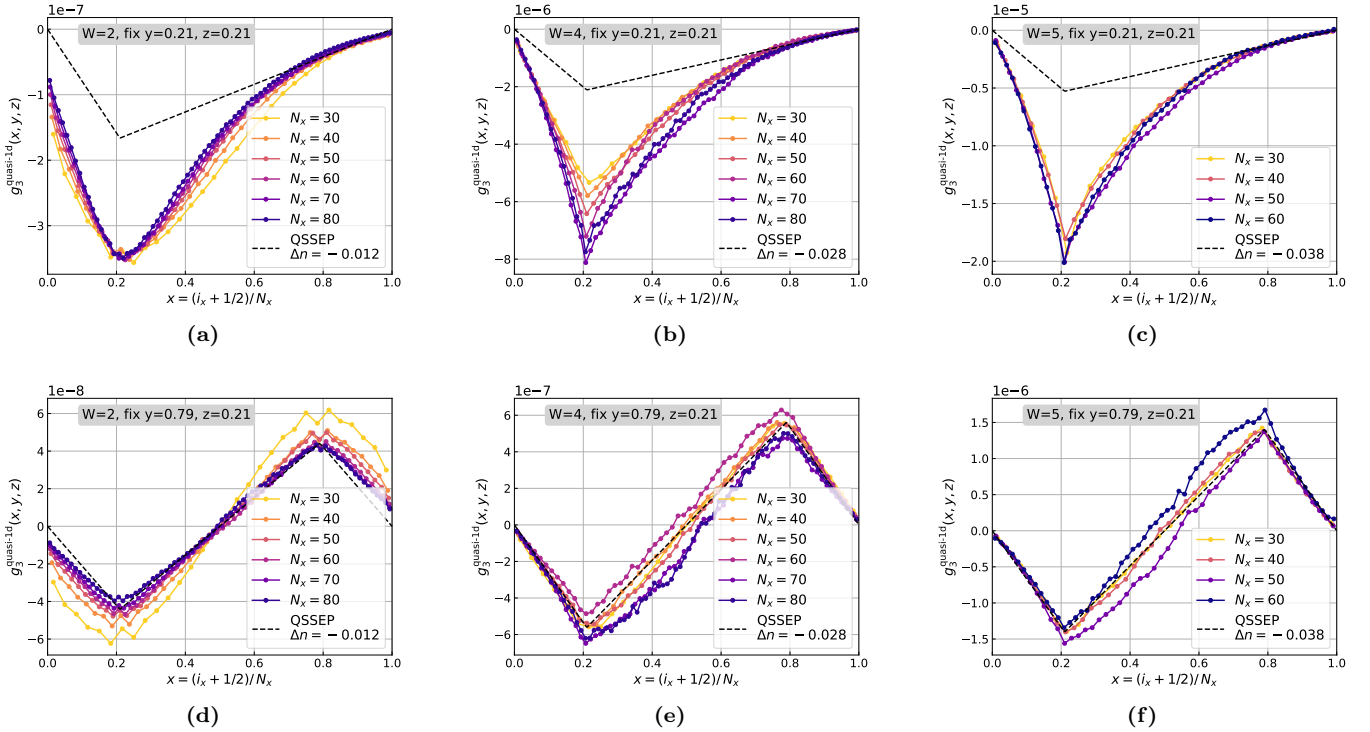


FIG. 7. Third cumulant $g_3^{\text{quasi-1d}}(x, y, z)$ in the quasi-1d Anderson model for $W = 2, 3, 5$ and with fixed transverse dimensions $N_y = N_z = 8$. In all plots the value of $z = i_z/N_x = 0.21$ is fixed together with $y = j_x/N_x = 0.21$ (in (a)-(c)) and $y = 0.79$ (in (d)-(f)). The value of Δn is fitted by hand to the latter. Note that the convergence with increasing N_x is better for lower values of W which is probably due to numerical errors. Indeed, for $W = 5$, $N_y = N_z = 8$ and $N_x > 60$ our numerical simulation diverges and we don't show these curves here. All data points are obtained as averages over 500 samples.

Results for varying disorder strength in the 3d case

In the main text we found the best correspondence of correlations g_n^Q in the 3d Anderson model with QSSEP for a disorder strength $W = 6$. In Figs. 8, 9 and 10, we show our results for two more values $W = 4$ and $W = 7$. Note that varying W has an effect on the extracted values of Δn . Furthermore, we observe that for fixed W , the values $\Delta n^{(1)}$ and $\Delta n^{(2)}$ fitted to the first and second cumulant only agree very approximately (best agreement for $W = 7$). But $\Delta n^{(3)}$ fitted to the third cumulant differs a lot and carries a negative sign which we don't know how to explain yet.

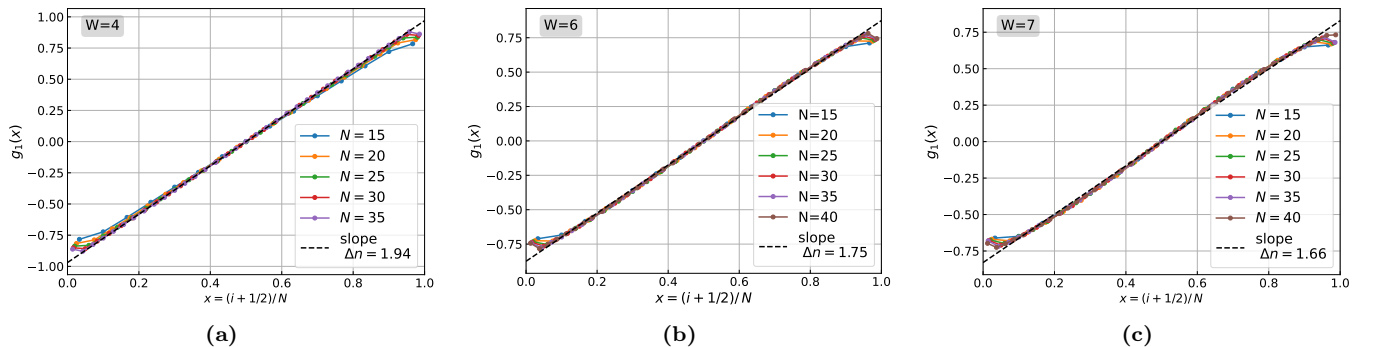


FIG. 8. The density $g_1(x)$ in the 3d Anderson model for $W = 4, 6, 7$. The imbalance $\Delta n^{(1)}$ seems to slightly decrease with increasing disorder W . Disorder averages are performed over 1000 realizations for every point.

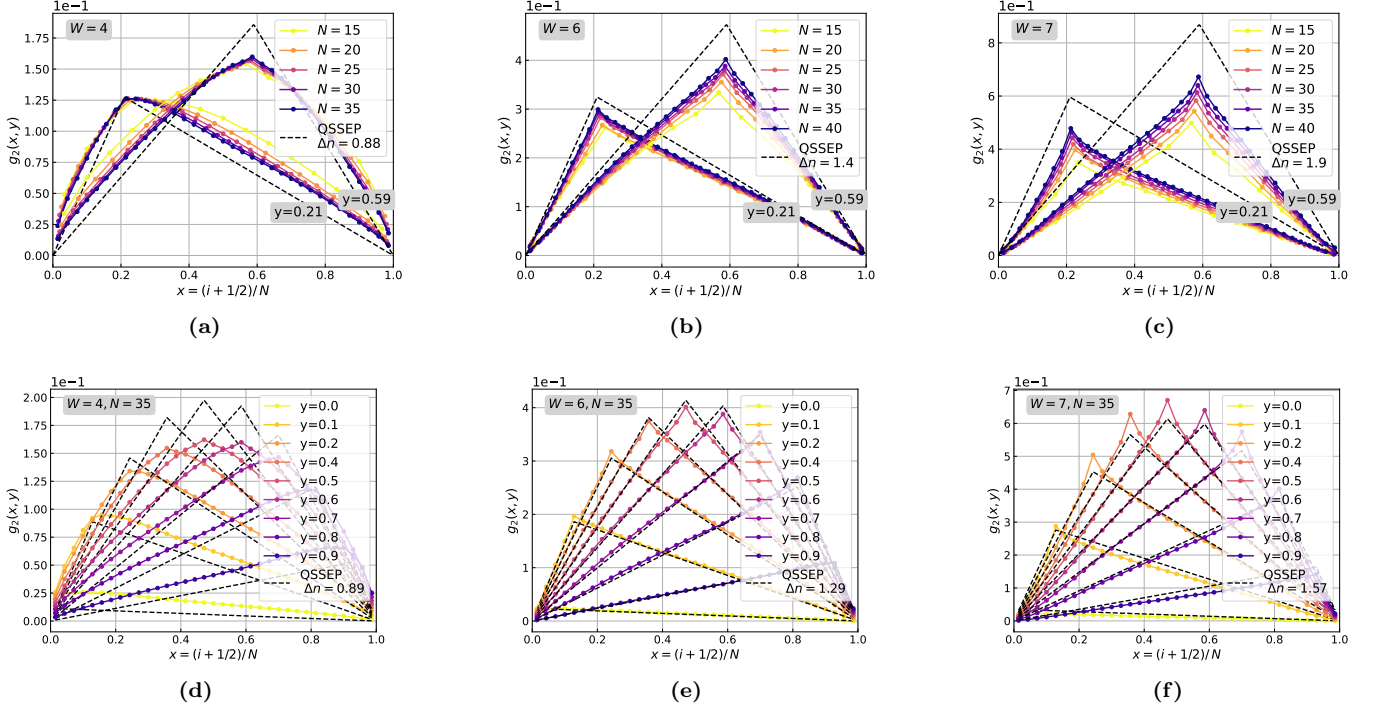


FIG. 9. Second cumulant $g_2(x, y)$ in the 3d Anderson model for $W = 4, 6, 7$. In (a)-(c) curves for two fixed values of $y = j_x/N_x = 0.21, 0.59$ and for different values of N are collapsed in order to show that the curves converge for large N for all values of W . The imbalance $\Delta n^{(2)}$ for the QSSEP prediction (dashed line) is found as the best fit to an extrapolation of the data to $N \rightarrow \infty$. In (d)-(f) curves correspond to $N = 35$ but at different values of y . Here the imbalance for the QSSEP prediction (dashed line) is obtained as the best fit to the data for $N = 35$ (and not for $N_x \rightarrow \infty$).

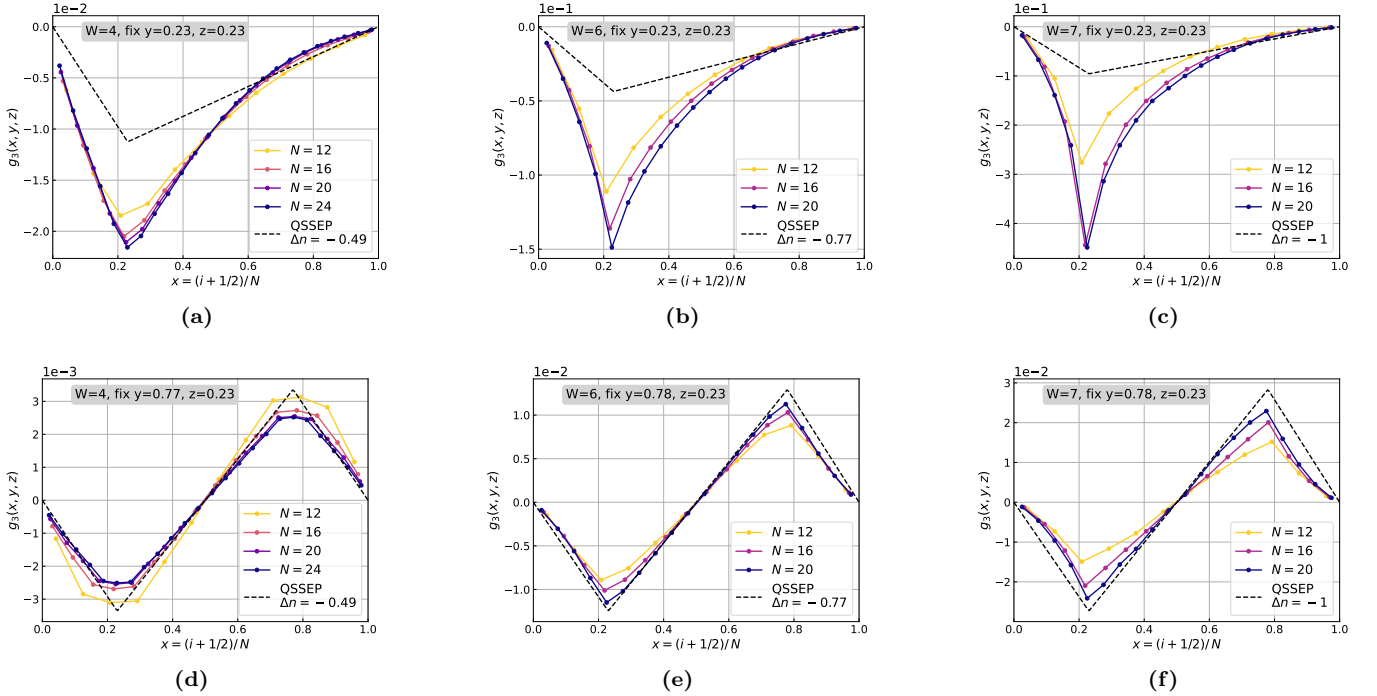


FIG. 10. Third cumulant $g_3(x, y, z)$ in the 3d Anderson model for $W = 4, 6, 7$. In all plots the value of $z = i_z/N_x = 0.21$ is fixed together with $y = j_x/N_x = 0.21$ (in (a)-(c)) and $y = 0.79$ (in (d)-(f)). For the latter, $\Delta n^{(3)}$ is fitted by hand.

Numerical methods for the Anderson model

For completeness, we recall explicitly the methodology here. We look for eigenmodes of the system that corresponds to incoming right or left movers from the reservoirs. A given eigenmode is characterized by its energy E and *incident* wave vector $\mathbf{k} = (k_x, k_\perp)$ where k_x is fixed by E and k_\perp through the dispersion relation $E_{\mathbf{k}} = -\sum_{\nu=x,y,z} 2t_\nu \cos(k_\nu a)$. Let $|\psi_{\alpha,E,k_\perp}\rangle$, $\alpha = \text{L,R}$ denotes such a single-particle state where L/R refers to incoming left/right modes. They fulfill the Schrödinger equation

$$H |\psi_{\alpha,E,k_\perp}\rangle = E |\psi_{\alpha,E,k_\perp}\rangle. \quad (16)$$

From this equation, we have a recursive way of relating the wave functions in a given slice j_x to $j_x + 1$. Explicitly:

$$\begin{pmatrix} \Psi_{j_x+1} \\ \Psi_{j_x} \end{pmatrix} = M_{j_x} \begin{pmatrix} \Psi_{j_x} \\ \Psi_{j_x-1} \end{pmatrix}. \quad (17)$$

where $\Psi_{j_x} = \{\psi_{j_x,j_\perp}\}_{j_\perp}$ is an vector with N^2 elements specifying the wave function at $\mathbf{j} = (j_x, j_\perp)$ and M_{j_x} is an $2N^2 \times 2N^2$ matrix defined as:

$$M_{j_x} = \begin{pmatrix} \frac{1}{t_x} (\mathcal{V}_{j_x} - E\mathbb{I} - \mathcal{T}) & -\mathbb{I} \\ \mathbb{I} & 0 \end{pmatrix} \quad (18)$$

where \mathcal{T} and \mathcal{V}_{j_x} are $N^2 \times N^2$ matrices whose elements are given by $\sum_{\nu \in \{y,z\}} t_\nu (\delta_{j_\nu, j'_\nu+1} + \delta_{j_\nu, j'_\nu-1})$ and $\delta_{j_y j'_y} \delta_{j_z j'_z} V_j$ respectively. In the clean regions, we can always decompose the wave function in the basis of plane waves:

$$\Psi_{j_x \in \text{L/R}} = \sum_{k_\perp} \frac{e^{ik_\perp \cdot j_\perp}}{N} (A_{\text{L/R}, k_\perp} e^{\pm ik_x j_x} + B_{\text{L/R}, k_\perp} \mp e^{ik_x j_x}). \quad (19)$$

where $k_\perp := (k_y, k_z)$, $j_\perp := (j_y, j_z)$. The previous relation to go from plane wave to position basis has a matrix formulation. For left incomers:

$$\begin{pmatrix} \Psi_{j_x+1} \\ \Psi_{j_x} \end{pmatrix} = Q_L(j_x) \begin{pmatrix} A_L \\ B_L \end{pmatrix}, \quad (20)$$

where $A_L = \{A_{L,k_\perp}\}_{k_\perp}$ and $B_L = \{B_{L,k_\perp}\}_{k_\perp}$ are N^2 vectors,

$$Q_L(j_x) = \begin{pmatrix} U_L & 0 \\ 0 & U_L \end{pmatrix} \begin{pmatrix} D_{j_x+1} & D_{j_x+1}^* \\ D_{j_x} & D_{j_x}^* \end{pmatrix} \quad (21)$$

where U_L and D_{j_x} are $N^2 \times N^2$ matrices with elements $U_{L,j_\perp,k_\perp} = \frac{e^{ik_\perp \cdot j_\perp}}{N}$ and $D_{j_x,k_\perp,k'_\perp} = \delta_{k_\perp,k'_\perp} e^{ik_x(j_x+1)}$ where we recall that k_x depends explicitly on (E, k_\perp) through the dispersion relation $E_{\mathbf{k}} = -\sum_{\nu=x,y,z} 2t_\nu \cos(k_\nu a)$.

The transfer matrix relates the amplitudes of the plane waves in the left reservoir to the ones in the right one:

$$\begin{pmatrix} B_R \\ A_R \end{pmatrix} = T \begin{pmatrix} A_L \\ B_L \end{pmatrix}, \quad (22)$$

Since the indices for A_R and B_R are swapped compared to A_L and B_L , we have in this convention that $Q_R = Q_L$ (see Eq. (19)) that we will simply note Q from now on. The explicit expression of T is

$$T = Q(N-1)^{-1} M_{N-1} \cdots M_0 Q(-1). \quad (23)$$

Let $T =: \begin{pmatrix} T_{11} & T_{12} \\ T_{21} & T_{22} \end{pmatrix}$ where T_{ij} are $N^2 \times N^2$ matrices. For a given right incomer associated to wave number k'_\perp and energy E , we fix $A_{R,k_\perp} := \frac{1}{\sqrt{2t_z \sin(k'_x)}} \delta_{k_\perp, k'_\perp}$ (we use the convention where the incoming current of a given mode is normalized to 1), take $A_L = 0$, and we have $B_L = T_{22}^{-1} A_R$. Finally, the elements of $|\psi_{R,E,k_\perp}\rangle$ in position space, can be built from the relation:

$$\begin{pmatrix} \Psi_{j_x+1} \\ \Psi_{j_x} \end{pmatrix} = M_{j_x} \cdots M_0 Q(-1) \begin{pmatrix} 0 \\ (T_{22})^{-1} A_R \end{pmatrix}, \quad (24)$$

This procedure allows us to obtain the elements of all the single-particle wave functions $|\psi_{\text{R},E,k_\perp}\rangle$ in position space.

For left incomers, the corresponding recursion relation is

$$\begin{pmatrix} \Psi_{N-1-j_x} \\ \Psi_{N-2-j_x} \end{pmatrix} = M_{N-1-j_x}^{-1} \cdots M_{N-1}^{-1} Q(N-1) \begin{pmatrix} (T^{-1})_{11}^{-1} A_L \\ 0 \end{pmatrix} \quad (25)$$

with the explicit expression for $M_{j_x}^{-1}$:

$$M_{j_x}^{-1} = \begin{pmatrix} 0 & \mathbb{I} \\ -\mathbb{I} & \frac{1}{t_x} (\mathcal{V}_{j_x} - E - \mathcal{T}) \end{pmatrix}. \quad (26)$$

The statistics of the bath is now incorporated by going to second quantization. Let $a_\alpha^\dagger(E, k_\perp)$ be the second quantized fermionic creation operator associated to $|\psi_{\alpha,E,k_\perp}\rangle$. We fix

$$\langle a_\alpha^\dagger(E, k_\perp) a_{\alpha'}(E', k'_\perp) \rangle = \delta_{\alpha\alpha'} \delta(E - E') \delta_{k_\perp, k'_\perp} f(E, T_\alpha, \mu_\alpha). \quad (27)$$

And the two-point function $G_{i,j}^A := \langle c_j^\dagger c_i \rangle$ whose statistics we are interested in is finally given by

$$G_{ij}^A = \int dE \sum_{\alpha=L,R} f(T_\alpha, \mu_\alpha, E) \sum_{k_\perp} \psi_{\alpha,E,k_\perp}^*(\mathbf{j}) \psi_{\alpha,E,k_\perp}(\mathbf{i}) \quad (28)$$

Imposing a small imbalance between the leads $\mu_{L/R} = \mp \delta\mu$ and fixing $T_L = T_R = 0$, we can expand around $E = 0$. Denoting $G_{ij}^\alpha(E) := \sum_{k_\perp} \psi_{\alpha,E,k_\perp}^*(\mathbf{j}) \psi_{\alpha,E,k_\perp}(\mathbf{i})$ we have

$$G^A \approx \delta\mu (G^{\text{R}}(0^+) - G^{\text{L}}(0^-)) + \int_{-\infty}^0 dE (G^{\text{R}}(E) + G^{\text{L}}(E)) \quad (29)$$

and one identifies the non-equilibrium part of G as

$$G^{\text{neq}} := \delta\mu (G^{\text{R}}(0^+) - G^{\text{L}}(0^-)), \quad (30)$$

where 0^\pm means that we can evaluate the energy for any point in the interval $[0, \pm\delta\mu]$ but should avoid taking the exact same point for the left and right movers as this is a special case. Throughout our simulations we took $0^\pm = \pm 0.2$. For convenience, we will avoid dealing with imaginary values for k_x by imposing an anisotropic tight-binding term: $t_y, t_z \ll \frac{1}{2}t_x$.

Renormalization procedure

In this section, we give more details on the renormalization procedure of the algorithm that was proposed in [27]. Due to the iterative application of M_{j_x} in the definition of the transfer matrix T in Eq. (23), the eigenvalues of the block T_{22} can become very small and can get lost numerically. However, these small eigenvalues dominate of the inverse T_{22}^{-1} . Therefore a renormalization procedure is necessary.

First, we introduce the notations $Q^{-1}(N-1) = \begin{pmatrix} L^+ \\ L^- \end{pmatrix}$ and $Q(-1) = (R^+|R^-)$ where L^\pm and R^\pm are $N \times 2N$ and $2N \times N$ matrices respectively. T_{22} is given by

$$T_{22} = L^- M_{N-1} \cdots M_0 R^- \quad (31)$$

which can be rewritten as $T_{22} = L^- r_{N-1}$ with $r_n = M_n r_{n-1}$ and $r_{-1} = R^-$. The top and bottom half

$$r_n = \begin{pmatrix} r_{1,n} \\ r_{2,n} \end{pmatrix} \quad (32)$$

tend to have large eigenvalues, hence the small eigenvalues relevant for the inversion of T_{22} will get lost in the iteration. To cure this problem, we define the $2N \times N$ matrix

$$r'_n := r_n (r_{1,n})^{-1} \quad (33)$$

such that each block has eigenvalues of order one. Then $(T_{22})^{-1}$ is expressed as

$$(T_{22})^{-1} = (r_{1,N-1})^{-1} (L^- r'_{N-1})^{-1}. \quad (34)$$

The algorithm to find r'_N is as follows:

- Initialize $r'_{-1} = R^-(R_1^-)^{-1}$
- Compute $\tilde{r}_n = M_n r'_{n-1}$ and $(\tilde{r}_{1,n})^{-1}$
- Multiply to get $r'_n = \tilde{r}_n (\tilde{r}_{1,n})^{-1}$ (note the relation $\tilde{r}_n = r_n r_{1,n-1}^{-1}$). This is the trick of the renormalization algorithm: We obtain r'_n without the need to calculate the bad conditioned r_n . Iterating, we get r'_{N-1} .
- From the relation $(\tilde{r}_{1,n})^{-1} = r_{1,n-1} (r_{1,n})^{-1}$ one deduces $(R_1^-)^{-1} (\tilde{r}_{1,1})^{-1} \cdots (\tilde{r}_{1,N-1})^{-1} = (r_{1,N-1})^{-1}$, from which we get $(r_{1,N})^{-1}$.

The renormalization procedure for $(T^{-1})_{11}$, which is necessary to treat left incomers, is obtained in a similar way.

$$(T^{-1})_{11} = L^+ M_0^{-1} \cdots M_{N-1}^{-1} R^+. \quad (35)$$

Rename the list $[M_{N-1}^{-1}, \cdots, M_0^{-1}] = [W_0, \cdots, W_{N-1}]$.

$$(T^{-1})_{11} = L^+ (-1) W_{N-1} \cdots W_0 R^+ \quad (36)$$

and we are back with the same situation than for T_{22} up to renaming of the object $M \rightarrow W$ and swapping $L^-/R^- \rightarrow L^+/R^+$.